

**Epitaxial growth of Fe<sub>3</sub>Si/CaF<sub>2</sub>/Fe<sub>3</sub>Si magnetic tunnel junction  
structures on CaF<sub>2</sub>/Si(111) by molecular beam epitaxy**

Ken'ichi Kobayashi<sup>a</sup>, Takashi Suemasu<sup>a</sup>, Noriyuki Kuwano<sup>b</sup>, Daisuke Hara<sup>b</sup> and

Hiroyuki Akinaga<sup>c</sup>

<sup>a</sup>*Institute of Applied Physics, University of Tsukuba, Tsukuba, Ibaraki 305-8573, Japan*

<sup>b</sup>*Department of Applied Science for Electronics and Materials, Kyushu University, 6-1*

*Kasuga, Fukuoka 816-8580, Japan*

<sup>c</sup>*Nanoelectronics Research Institute, National Institute of Advanced Industrial Science  
and Technology, Tsukuba, Ibaraki 305-8568, Japan*

The Fe<sub>3</sub>Si(24 nm)/CaF<sub>2</sub>(2 nm)/Fe<sub>3</sub>Si(12 nm) magnetic tunnel junction (MTJ) structures were grown epitaxially on CaF<sub>2</sub>/Si(111) by molecular beam epitaxy (MBE). The 12-nm-thick Fe<sub>3</sub>Si underlayer was grown epitaxially on CaF<sub>2</sub>/Si(111) at approximately 400°C; however, the surface of the Fe<sub>3</sub>Si film was very rough, and thus a lot of pinholes are considered to exist in the 2-nm-thick CaF<sub>2</sub> barrier layer. The average roughness (Ra) of the CaF<sub>2</sub> barrier layer was 7.8 nm. This problem was overcome by low temperature deposition of Fe and Si at 80°C on CaF<sub>2</sub>/Si(111), followed by

annealing at 250°C for 30 min to form the Fe<sub>3</sub>Si layer. The Ra roughness was significantly reduced down to approximately 0.26 nm. A hysteresis loop with coercive field  $H_c$  of approximately 25 Oe was obtained in the magnetic field dependence of Kerr rotation at room temperature (RT).

KEYWORDS: ferromagnetism, Fe<sub>3</sub>Si, CaF<sub>2</sub>, Si

**Corresponding author:** Prof. T. Suemasu, Institute of Applied Physics, University of Tsukuba, Tsukuba, Ibaraki 305-8573, Japan.

TEL(FAX): +81-29-853-5111, Email: suemasu@bk.tsukuba.ac.jp

## 1. Introduction

In recent years, magnetic materials have been developed to be used in magnetic tunnel junctions (MTJs). They consist of two ferromagnetic electrodes separated by a barrier layer, and show the tunnel magnetoresistance (TMR) effect [1,2]. This phenomenon has been applied to magnetoresistive random access memory (MRAM). Since an MRAM has been proposed as a universal memory [3], in which not only high-speed operation in a static random-access memory (SRAM) but also high integrity in a dynamic random-access memory (DRAM) can be expected. In order to achieve Gb-scale MRAM, TMR ratios exceeding 150% and higher output voltages ( $>190$  mV) are required [4]. However, the TMR ratio of current MTJs with an amorphous barrier layer is approaching its theoretical limit. One way to overcome these difficulties is to use fully epitaxial MTJs together with highly spin-polarized ferromagnetic electrodes. We think that ferromagnetic  $\text{Fe}_3\text{Si}$  is a good candidate for such a material.  $\text{Fe}_3\text{Si}$  is ferromagnetic up to  $530\text{-}570^\circ\text{C}$  [5-7], and it possesses two distinct Fe sites with magnetic moments  $\mu_{\text{Fe}^{\text{I}}}=2.2 \mu_{\text{B}}/\text{atom}$  and  $\mu_{\text{Fe}^{\text{II}}}=1.35 \mu_{\text{B}}/\text{atom}$ , where  $\mu_{\text{B}}$  is the Bohr magneton. Thus,  $\text{Fe}_3\text{Si}$  can be regarded as a Heusler alloy  $\text{Fe}^{\text{II}}_2\text{Fe}^{\text{I}}\text{Si}$ , ( $\text{DO}_3$  type) [8], and therefore a candidate for being half-metallic [9].  $\text{Fe}_3\text{Si}$  has a lattice parameter of  $0.564$  nm, which is nearly lattice-matched to Si. Very recently,

the epitaxial growth of Fe<sub>3</sub>Si on Si(111) was reported [10]. However, it is difficult to prevent the formation of interfacial compounds like FeSi due to the diffusion of Si atoms from the substrate into the grown films [11], which is unfavorable for large TMR ratios. To avoid this problem, we inserted CaF<sub>2</sub> layers between Fe<sub>3</sub>Si and Si substrates. CaF<sub>2</sub> is known to grow epitaxially on Si(111) substrates at temperatures higher than 600°C [12-14]. We have realized the epitaxial growth of Fe<sub>3</sub>Si on CaF<sub>2</sub>/Si(111) by molecular beam epitaxy (MBE) [11,15].

The purpose of this investigation was to form Fe<sub>3</sub>Si/CaF<sub>2</sub>/Fe<sub>3</sub>Si TMR structures epitaxially on CaF<sub>2</sub>/Si(111) by MBE. Surface roughness and magnetic properties of the grown layers were also investigated.

## **2. Experimental**

An ion-pumped MBE system equipped with electron-beam evaporation sources for Fe and Si was used. CaF<sub>2</sub> was evaporated by a high-temperature Knudsen cell. The Fe<sub>3</sub>Si(24 nm)/CaF<sub>2</sub>(2 nm)/Fe<sub>3</sub>Si(12 nm) TMR structures were epitaxially grown on CaF<sub>2</sub>/Si(111) by MBE as follows: first, a 50-nm-thick Si buffer layer was grown at 450°C on Si(111) substrates. Then, wafers were annealed at 1000°C for 30 min to improve the crystal quality. Next, 8-nm-thick CaF<sub>2</sub> was grown epitaxially on Si(111) at

600°C. Then, Si and Fe were co-evaporated at 400°C to form a 12-nm-thick Fe<sub>3</sub>Si first layer, followed by a 2-nm-thick CaF<sub>2</sub> barrier layer grown at 600°C. Finally, a 24-nm-thick Fe<sub>3</sub>Si 2nd layer was grown in the same manner. This sample is denoted as sample A. For comparison, the CaF<sub>2</sub>/Fe<sub>3</sub>Si/CaF<sub>2</sub> structure was grown at a low temperature as follows: after the growth of a 50-nm-thick Si buffer layer, 8-nm-thick CaF<sub>2</sub> was grown epitaxially on Si(111) at 600°C. Then, Si and Fe were co-evaporated at a low temperature of 80°C, and then annealed at 250°C for 30 min to form 20-nm-thick Fe<sub>3</sub>Si. Finally, 2-nm-thick CaF<sub>2</sub> was grown at 280°C. This sample is denoted as sample B. The deposition rates of Si and Fe were kept constant at 4.0 and 2.2 nm/min, respectively. They were determined using the theoretical densities of Fe and Si to satisfy stoichiometry in Fe<sub>3</sub>Si.

The crystalline quality of the grown films was characterized by reflection high-energy electron diffraction (RHEED) and  $\theta$ -2 $\theta$  X-ray diffraction (XRD). RHEED patterns were observed along the [1-10] azimuth of the Si. The surface morphology was investigated using atomic force microscopy (AFM). Magneto-optical Kerr effect (MOKE) was measured to obtain the hysteresis loop of the Kerr rotation using a 632.8 nm He-Ne laser with the magnetic field up to 1500 Oe in the film plane along the [1-10] direction of Fe<sub>3</sub>Si.

### 3. Results and discussion

#### 3.1 High-temperature growth of $Fe_3Si$

Figure 1 shows RHEED patterns of each stage of sample A. Figure 1(a) was taken after the thermal cleaning of the substrate. Figures 1(b-e) show RHEED patterns of the 8-nm-thick  $CaF_2$  first layer, the 12-nm-thick  $Fe_3Si$  first layer, the 2-nm-thick  $CaF_2$  barrier layer and the 24-nm-thick  $Fe_3Si$  second layer, respectively. Streaky RHEED pattern was observed in every stage. These results indicate that the  $Fe_3Si/CaF_2/Fe_3Si$  MTJ structure was epitaxially grown on  $CaF_2/Si(111)$ , although small amount of  $FeSi$  was included as shown in the  $\theta$ - $2\theta$  XRD pattern of Fig. 2. Since the growth temperature of the  $CaF_2$  second layer is much higher than  $400^\circ C$ , it is considered to be difficult to prevent formation of  $FeSi$  as shown in our previous paper [11]. As shown in Fig. 3, a hysteresis loop was observed at RT in the magnetic field dependence of Kerr rotation. However, a step-like hysteresis loop, which exhibits the difference in coercive field  $H_c$  between the two ferromagnetic  $Fe_3Si$  layers, was not observed. This means that the two layers are ferromagnetically coupled. Figure 4 shows the  $2 \times 2\text{-}\mu m^2$ -area AFM top view and cross-sectional profile of sample A. It was found that the surface of sample A was very rough; the average roughness Ra was 7.8 nm. This roughness is attributed to the

rough surface of the  $\text{Fe}_3\text{Si}$  first layer as shown in Fig. 5. Figure 5 shows a typical example of the  $2 \times 2\text{-}\mu\text{m}^2$ -area AFM top view and cross-sectional profile taken after the growth of the 12-nm-thick  $\text{Fe}_3\text{Si}$  first layer in sample A. The Ra roughness already reaches 2.9 nm at this stage. We therefore speculate that there exist lots of pinholes in the 2-nm-thick  $\text{CaF}_2$  barrier layer through which the two ferromagnetic  $\text{Fe}_3\text{Si}$  layers may contact. Thus, the formation of an  $\text{Fe}_3\text{Si}$  first layer with atomically flat surface is mandatory.

### *3.2 Low-temperature growth of $\text{Fe}_3\text{Si}$*

In order to obtain  $\text{Fe}_3\text{Si}$  films with flat surface, we attempted low-temperature formation of  $\text{Fe}_3\text{Si}$ . Figure 6 shows RHEED patterns of each stage of sample B. Fig. 6(a) was taken after the thermal cleaning of the substrate. Fig. 6(b-e) are RHEED patterns taken after the growth of the 8-nm-thick  $\text{CaF}_2$  first layer, after codeposition of Fe and Si at  $80^\circ\text{C}$ , after the subsequent annealing at  $250^\circ\text{C}$  for 30 min, and after the growth of the 2-nm-thick  $\text{CaF}_2$  second layer at  $280^\circ\text{C}$ , respectively. As shown in Fig. 6(c), just after the codeposition of Si and Fe at  $80^\circ\text{C}$ , spotty RHEED pattern was observed, meaning crystalline  $\text{Fe}_3\text{Si}$  was formed even at such a low temperature. Because of the low-temperature, the surface migration of deposited Fe and Si atoms was limited, thus resulting in the spotty RHEED pattern. This spotty pattern changed into

streaky after annealing at 250°C as shown in Fig. 6(d), meaning that the rough surface was flattened. After the growth of the CaF<sub>2</sub> second layer at 280°C, a streaky pattern was also observed as shown in Fig. 6(e); however, it seems spotty and diffused compared to the RHEED pattern of the 2-nm-thick CaF<sub>2</sub> layer grown at 600°C shown in Fig. 1(d). This was caused by the low-temperature formation of the CaF<sub>2</sub> layer. Fig. 7 shows the 2×2-μm<sup>2</sup>-area AFM top view and cross-sectional profile of sample B. We should note that sample B has a very smooth surface with Ra roughness=0.26 nm. The difference in the surface morphology between samples A and B is attributed to the difference in the growth temperature of the Fe<sub>3</sub>Si first layer. A hysteresis loop is clearly seen in the magnetic field dependence of Kerr rotation as shown in Fig. 8. The coercive field  $H_c$  was approximately 25 Oe. By forming another Fe<sub>3</sub>Si layer epitaxially on sample B, fully epitaxial MTJs together with highly spin-polarized half-metallic ferromagnetic electrodes will be obtained in the near future.

#### **4. Conclusion**

We have realized the epitaxial growth of Fe<sub>3</sub>Si(24 nm)/CaF<sub>2</sub>(2 nm)/Fe<sub>3</sub>Si(12 nm) MTJ structures on CaF<sub>2</sub>/Si(111) by MBE. However, the Ra roughness of the surface is approximately 7.8 nm. The rough surface was attributed to the surface

roughness of the Fe<sub>3</sub>Si first layer (Ra=2.9 nm). In order to overcome this problem, Fe<sub>3</sub>Si was formed by low-temperature codeposition of Fe and Si at 80°C, followed by 250°C annealing for 30 min. The surface morphology was greatly improved and the Ra roughness was deduced down to approximately 0.26 nm.

### **Acknowledgements**

This work was supported in parts from the Ministry of Education, Culture, Sports, Science and Technology (MEXT) of Japan.

## References

- [1] T. Miyazaki, N. Tezuka, *J. Magn. Magn. Mater.* **139** (1995) L231.
- [2] J. S. Moodera, L. R. Kinder, T. M. Wong, and R. Meservey, *Phys. Rev. Lett.* **74** (1995) 3273.
- [3] R. E. Fontana, S. R. Hetzler, *J. Appl. Phys.* **99** (2006) 08N902.
- [4] S. Yuasa, A. Fukushima, T. Nagahama, K. Ando, Y. Suzuki, *Jpn. J. Appl. Phys., Part 2* **43** (2004) L588.
- [5] A. Ôsawa, T. Murata, *Nippon Kinzoku Gakkai-Shi* **4** (1940) 228.
- [6] M. Hong, H. S. Chen, J. Kwo, A. R. Kortan, J. P. Mannaerts, B. E. Weir, L. C. Feldman, *J. Cryst. Growth* **111** (1991) 984.
- [7] J. Waliszewski, L. Dobrzyński, A. Malinowski, D. Satuła, K. Szymański, W. Prandl, Th. Brückel, O. Schärpf, *J. Magn. Magn. Mater.* **132** (1994) 349.
- [8] W. A. Hines, A. H. Menotti, J. I. Budnick, T. J. Burch, T. Litrenta, V. Niculescu, K. Raj, *Phys. Rev. B* **13** (1976) 4060.
- [9] R. A. de Groot, F. M. Mueller, P. C. Van Engen, K. H. Buschow, *Phys. Rev. Lett.* **50** (1983) 2024.
- [10] T. Sadoh, H. Takeuchi, K. Ueda, A. Kenjo, M. Miyao, *Jpn. J. Appl. Phys., Part 1* **45** (2006) 3598.

- [11] T. Sunohara, K. Kobayashi, M. Umada, H. Yanagihara, E. Kita, H. Akinaga, T. Suemasu, *Jpn. J. Appl. Phys., Part 2* **44** (2005) L715.
- [12] H. Ishirwara, T. Asano, *Appl. Phys. Lett.* **40** (1982) 66.
- [13] R.W. Fathauer, L.J. Schowater, *Appl. Phys. Lett.* **45** (1984) 519.
- [14] C. A. Lucas, D. Loretto, G. C. L. Wong, *Phys. Rev. B* **50** (1994) 14340.
- [15] K. Kobayashi, T. Sunohara, M. Umada, H. Yanagihara, E. Kita, T. Suemasu, *Thin Solid Films* **508** (2006) 78.

## Figure captions

Figure 1 RHEED patterns of each stage of sample A. (a) was taken after the thermal cleaning of the substrate. (b), (c), (d) and (e) show RHEED patterns of the 8-nm-thick CaF<sub>2</sub> first layer, the 12-nm-thick Fe<sub>3</sub>Si first layer, the 2-nm-thick CaF<sub>2</sub> barrier layer and the 24-nm-thick Fe<sub>3</sub>Si second layer.

Figure 2  $\theta$ -2 $\theta$  XRD pattern of sample A.

Figure 3 Magnetic field dependence of Kerr rotation obtained at RT for sample A in longitudinal geometry.

Figure 4 AFM top view and cross-sectional profile of sample A.

Figure 5 AFM top view and cross-sectional profile of the 12-nm-thick Fe<sub>3</sub>Si first layer in sample A.

Figure 6 RHEED patterns of each stage of sample B. (a) was taken after thermal cleaning of the substrate. (b), (c), (d) and (e) are RHEED patterns taken after the growth of the 8-nm-thick  $\text{CaF}_2$  first layer, after codeposition of Fe and Si at  $80^\circ\text{C}$ , after annealing at  $250^\circ\text{C}$  for 30min, and after the growth of the 2-nm-thick  $\text{CaF}_2$  second layer at  $280^\circ\text{C}$ , respectively.

Figure 7 AFM top view and cross-sectional profile of sample B.

Figure 8 Magnetic field dependence of Kerr rotation obtained for sample B at RT.

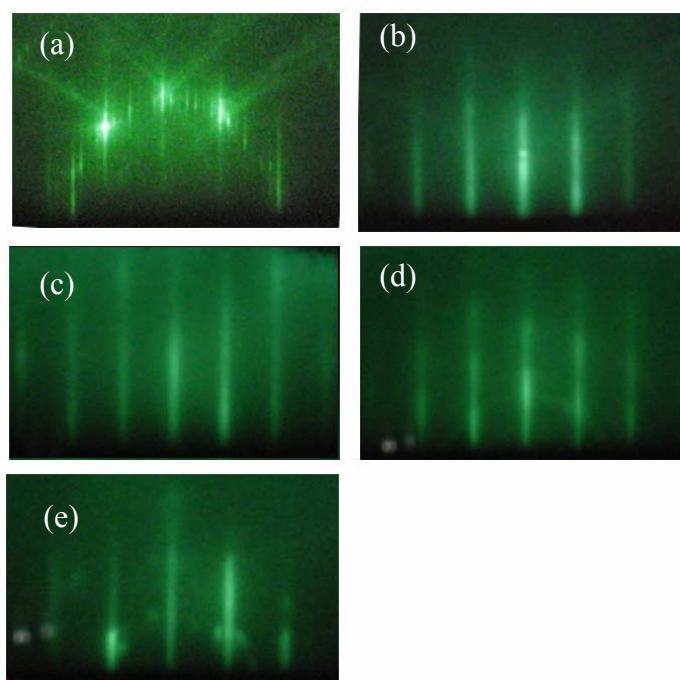


Fig. 1 Kobayashi *et al.*

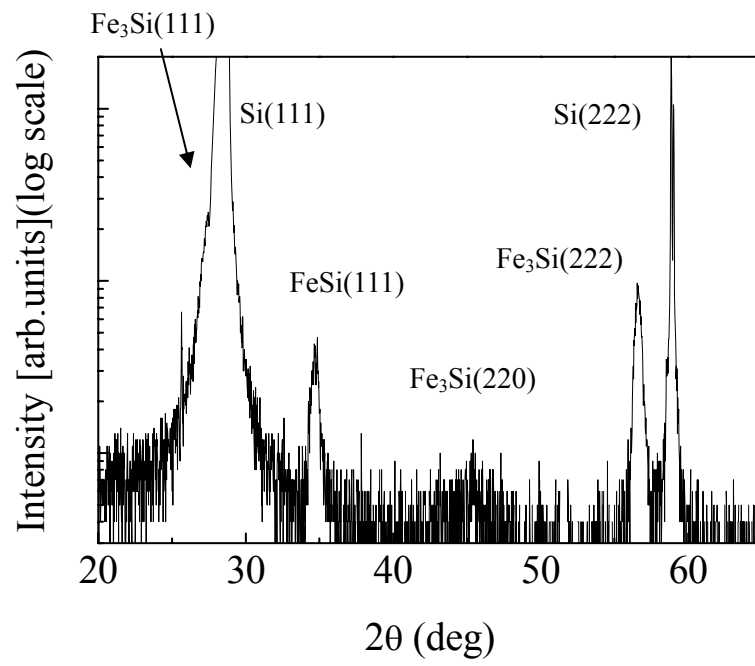


Fig. 2 Kobayashi *et al.*

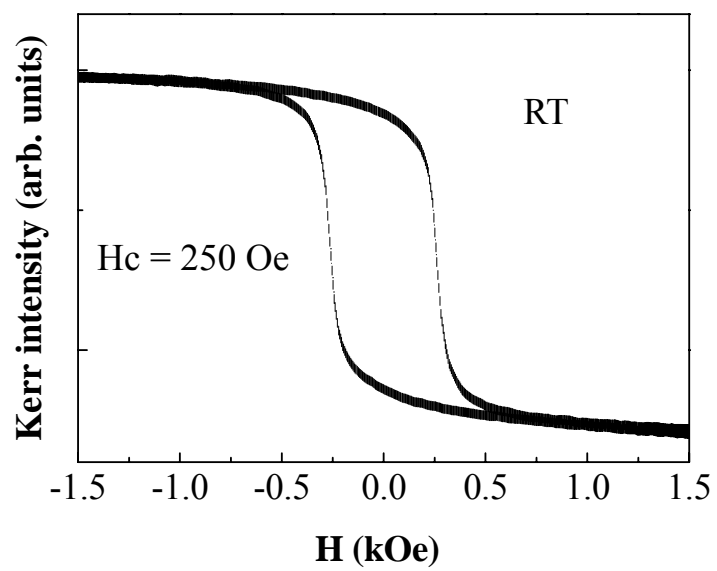


Fig. 3 Kobayashi *et al.*

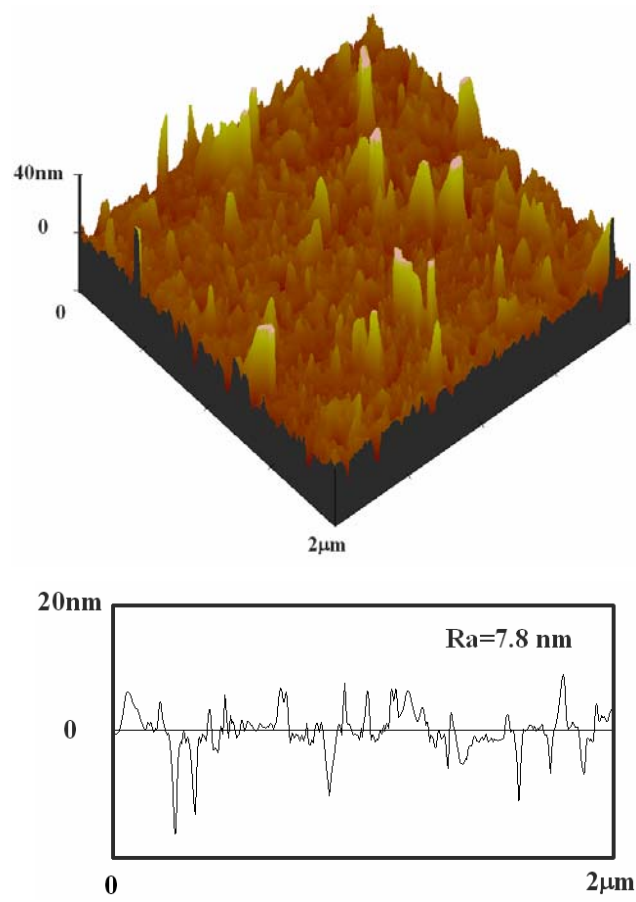


Fig. 4 Kobayashi *et al.*

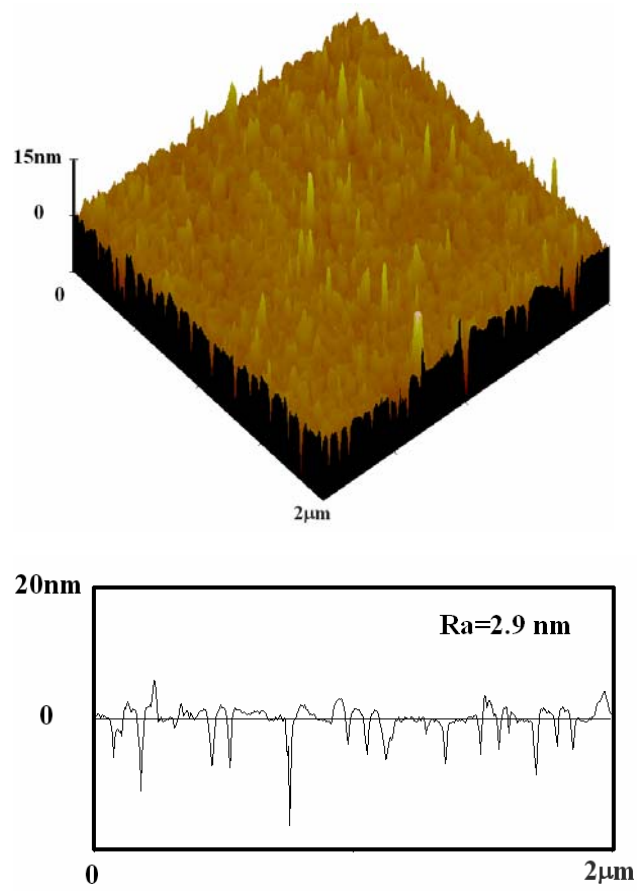


Fig. 5 Kobayashi *et al.*

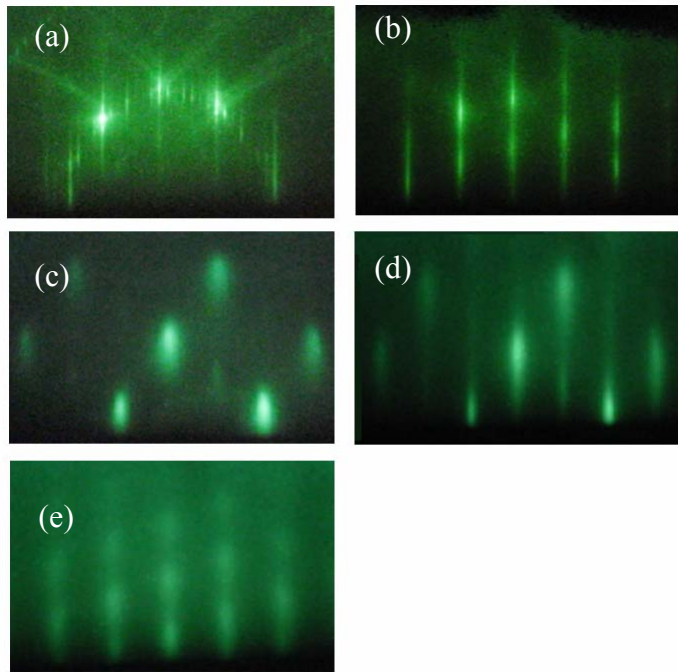


Fig. 6 Kobayashi *et al.*

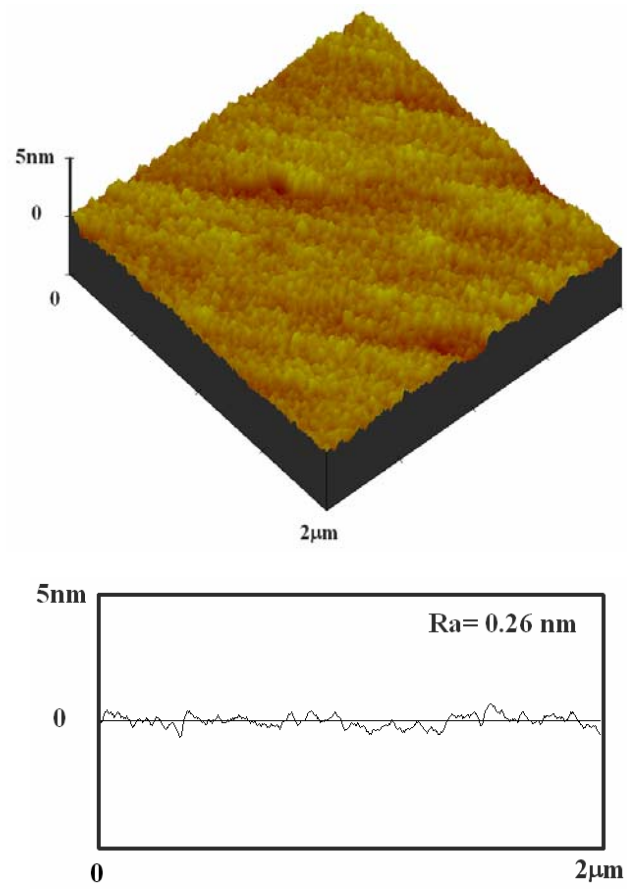


Fig. 7 Kobayashi *et al.*

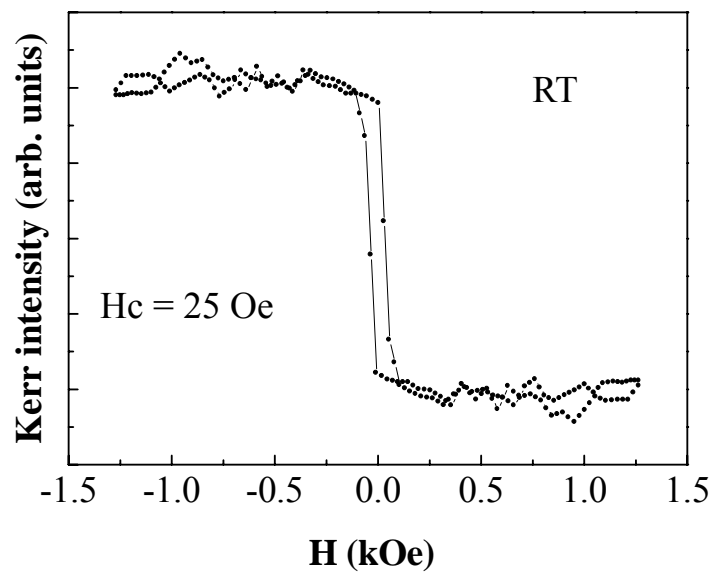


Fig. 8 Kobayashi *et al.*